




Article

New Glass Ceramic Materials Obtained from Cathode Ray Tubes Glass Wastes and Fly Ash

Cosmin Vancea, Giannin Mosoarca , Simona Popa , Mircea Dan  and Sorina Boran

Faculty of Industrial Chemistry and Environmental Engineering, Politehnica University Timisoara, Bd. V. Parvan, No. 6, 300223 Timisoara, Romania

* Correspondence: giannin.mosoarca@upt.ro (G.M.); mircea.dan@upt.ro (M.D.);
Tel.: +40-256-404-185 (G.M.); +40-256-404-176 (M.D.)

Abstract: This paper presents an alternative way to recycle cathode ray tube glass waste, together with fly ash and kaolin, into new glass ceramic materials. The samples were obtained using three firing temperatures: 700, 800, and 900 °C. The effect of the fly ash/CRT waste ratio upon the materials' firing shrinkage, apparent density, apparent and total porosity, chemical stability, and compression strength was investigated. The firing shrinkage used as a dimensional stability parameter, a firing shrinkage range between 2.19–8.18%, was positively influenced by the waste mix amount. The apparent density of the obtained materials is positively affected by the heat treatment temperature, rising from 2.09 to 2.93 (g·cm⁻³), while the apparent porosity decreases with the increase of the firing temperature from 6.08 to 2.24 %. All the studied glass ceramics show very good chemical stability and complete immobilization of the Pb²⁺ and Ba²⁺ ions in the glass ceramic matrix. The compression strength of the sintered materials ranges between 1.42–11.83 (N·mm⁻²), being positively influenced by the kaolin amount and negatively influenced by porosity. The obtained results confirm the viability of the proposed alternative to use CRT waste and fly ash together with kaolin to obtain glass ceramic materials that can be used for outdoor paving applications.

Keywords: cathode ray tube; fly ash; glass ceramics



Citation: Vancea, C.; Mosoarca, G.; Popa, S.; Dan, M.; Boran, S. New Glass Ceramic Materials Obtained from Cathode Ray Tubes Glass Wastes and Fly Ash. *Sustainability* **2023**, *15*, 3021. <https://doi.org/10.3390/su15043021>

Academic Editors: Valentina Colla and Ismael Matino

Received: 13 January 2023

Revised: 31 January 2023

Accepted: 3 February 2023

Published: 7 February 2023



Copyright: © 2023 by the authors. Licensee MDPI, Basel, Switzerland. This article is an open access article distributed under the terms and conditions of the Creative Commons Attribution (CC BY) license (<https://creativecommons.org/licenses/by/4.0/>).

1. Introduction

The electronics industry is one of the global industries with the fastest level of development, rapidly integrating new ideas and technologies and generating jobs but also a huge amount of e-waste [1]. The products of this industry have entered the daily life of members of today's society at all levels. Extremely rapid technological advances have generated a large number of early obsolete electronics, even if they are far from having completed their life cycles [2]. The combination of these two factors, increasing ownership and shortened lifespan, has generated rapid growth in the amount of unwanted and obsolete e-wastes, which exceeded 52 million tons in 2021 [3] and equals approximately 6.8 kg per inhabitant [4]. The e-waste contains more than 1000 different substances and up to 60 elements from the periodic table [5], many of which are toxic to human health and the environment. Their release to the environment generates a severe over-concentration of heavy metals in air, dust, soil, sediments, and plants, being a real danger to human health [6,7]. E-waste is one of the most problematic waste streams in terms of recycling and potential pollution [8]. Usually, household generated e-waste is collected either by dumping it into waste bins, through government-recognized collectors, or by private waste dealers and companies [9]. Recycling represents a profit-generating alternative for the economy, taking into account the content of precious metals (such as platinum, gold, silver, iridium, rhodium, etc.) and other marketable materials (copper, aluminum, indium, germanium, etc.) [10].

The technological evolution of displays from those with cathode ray tubes to thin-film transistors (TFTs), liquid crystal displays (LCDs), and the most advanced light-emitting

diodes (LEDs), and active-matrix organic light-emitting diodes (AMOLEDs) generates more than 50,000–150,000 million tons/year of CRT waste [11]. Stockpiling CRT e-waste from televisions and computer monitors is complicated due to their environmentally hazardous character derived from the large amounts of leaded glass they contain. Therefore, effective recycling alternatives must be proposed for these difficult-to-treat e-wastes. Two main approaches to CRT recycling are currently used: closed-loop and open-loop recycling [12]. The closed-loop alternative that involves the recovery of CRT waste as raw materials to manufacture new CRT monitors is currently obsolete since there is no more demand for CRT monitors from the market, and therefore, the recycling efforts shifted to open-loop recycling. Several main directions of open-loop recycling, each with specific advantages and disadvantages, have gained greater interest among researchers and manufacturers. CRT waste recycling by vitrification as an energy-consuming process is economically viable only by generating new glass-based products with high market value, such as cellular glasses [13–16], glass ceramics [17–20], ceramic glazes [21–24], and composites [25–28]. Another recycling trend that avoids the economic disadvantages associated with vitrification is for construction and infrastructure industries as a substitute for aggregates in cementitious matrices for concretes and mortars [29–35].

Fly ash is a by-product of power and incineration plants operated either on coal, biomass, or municipal solid waste. Fly ash, one of the most complex and abundant anthropogenic materials, is now considered the world's fifth-largest material resource [36]. Depending on its origins, the fly ash composition is very variable, and therefore, pollutants can be very different. It can generate water and soil pollution, disrupt ecological cycles, pose environmental hazards, and endanger human health if not properly stored. In most cases, the disposal of the ash is finally done by dumping it on open land [37]. Fine fly ash particles suspended in the air have become a major source of gas pollution, causing eye, skin, nose, throat, and respiratory tract irritation. When seeping into the basement, fly ash can clog natural drainage systems and contaminate groundwater with heavy metals. Considering the huge amounts of fly ash that are continuously generated, substantial efforts are required to find recycling alternatives. About 20% of fly ash is used in concrete production [38–41]. The physicochemical properties of coal fly ash, such as low bulk density, water-holding capacity, favorable pH, and useful nutrients, such as P, S, K, Ca, Mg, Cu, Mn, and Zn, make it a potential amendment for soils [42–44]. Fly ash can be used to stabilize the soil embankment, as an aggregate filler, as an additive for bituminous paving, and as a mineral filler for bituminous concrete for road base construction [45–47]. Based on its oxidic composition, containing mainly SiO_2 , Al_2O_3 , CaO , and Fe_2O_3 , and its fine powder form, which is able to be directly incorporated into ceramic pastes, fly ash is largely used in the ceramic industry [48–55]. Other fly ash applications include zeolite synthesis [56–58] and polymer fillers [59–61].

Although the application fields mentioned above use a good part of the generated fly ash, they are not sufficient for the complete recycling of the fly ash amounts.

Vitrification as a solution for ash immobilization and, respectively, for immobilizing CRT-type waste is the subject of recent studies that pursue the valorization of the products obtained in areas such as mortars [62], ceramic foams [63,64], porous glass ceramics [65], etc. This paper suggests a new recycling alternative using a lower-than-usual temperature firing for both CRT waste and fly ash, together with kaolin, to obtain new materials able to immobilize the barium and lead ions brought by the glass waste in the glass ceramic matrix. The materials' physicochemical properties recommend these materials for outdoor pavement applications.

2. Materials and Methods

The precursors' waste composition, which was determined using a RX fluorescence Niton XL 3 equipment (Thermo Fisher Scientific Inc., Waltham, MA, USA) for CRT and the fly ash and provided by the kaolin supplier SC IPEC SA (Alba Iulia, Romania), is presented in Table 1. Bojidar kaolin was introduced with the aim of ensuring, after the heat

treatment, the formation of the ceramic component of the synthesized samples, the essential component through the prism of the effect of the ceramic bridges on the properties of the final product. The kaolin phase composition is illustrated by the RDX spectra presented in Figure S1 (Supplementary Material).

Table 1. The precursors' oxidic composition (weight %).

Oxide	SiO ₂	Na ₂ O	K ₂ O	CaO	MgO	Al ₂ O ₃	Fe ₂ O ₃	BaO	PbO	TiO ₂	L.O.I
CRT	60.92	8.96	7.44	0.67	0.14	2.07	0.15	10.80	8.85	-	-
Fly ash	46.20	6.23	4.17	8.60	3.30	23.20	8.10	-	-	-	0.20
Bojidar kaolin	49.29	0.14	0.87	0.56	0.44	35.18	0.78	-	-	0.43	12.31

The glass waste was ground in a Pulverisette-type laboratory mill (Fritsch GmbH, Idar-Oberstein, Germany) using a material-balls-water ratio of 1:2:1, dried in an oven at 105 °C for 24 h, and then sieved, retaining the granulometric fraction under 100 µm mesh for later use.

The fly ash was provided by SC Colterm S.A. (Timisoara, Romania) powerplant. Its specific surface was determined by nitrogen adsorption (BET method) after prior degassing at 450 °C on a Micrometrix ASAP2020 porosimeter (Micromeritics, 4356 Communications Dr, Norcross, GA 30093, USA), was 6.3 (m²·g). The phase composition of the fly ash is presented in Figure S2 (Supplementary Material).

The particle size of the kaolin and fly ash was determined using a Micromeritics SediGraph III Plus particle size analyzer (Micromeritics, 4356 Communications Dr, Norcross, GA 30093, USA), using 2.5 g of each test sample. Once the testing was completed, the data was plotted, and the average fly ash and kaolin particle sizes (D50) were calculated as 17.25 µm and 6.78 µm, respectively (Figure 1).

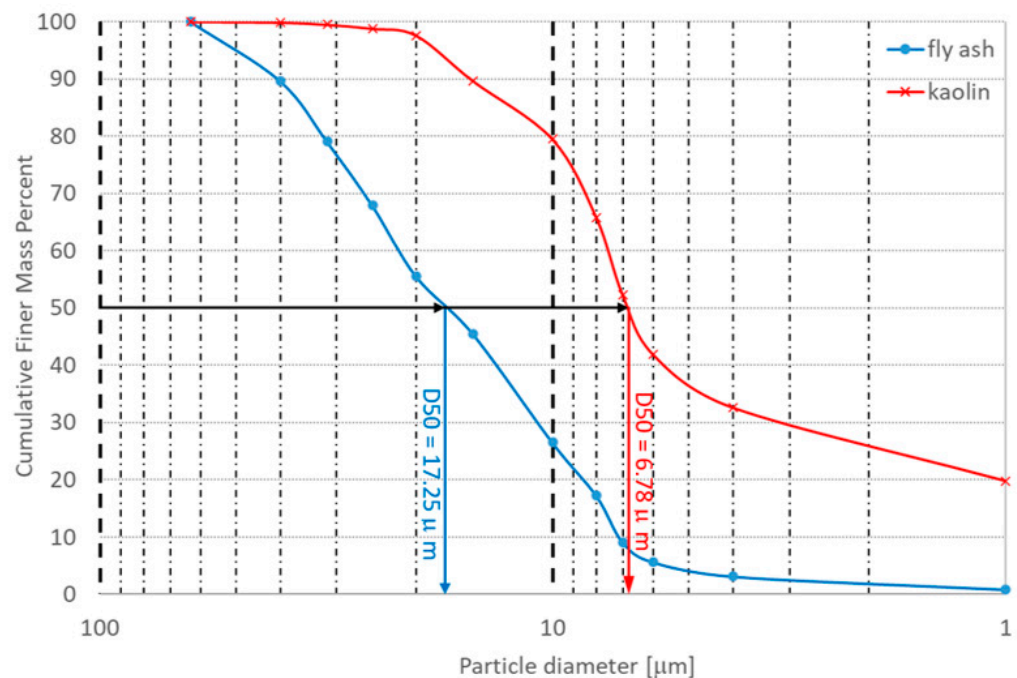


Figure 1. Particle size distribution of fly ash and Bojidar kaolin.

The compositions of the synthesized glass ceramics are presented in Table 2.

Table 2. Composition (weight %) and wastes ratio of the obtained glass ceramics.

Sample	Fly Ash	CRT Waste	Bojidar Kaolin	Fly Ash/CRT Ratio
1	20.00	40.00	40.00	0.50
2	30.00	35.00	35.00	0.86
3	40.00	30.00	30.00	1.33
4	50.00	25.00	25.00	2.00
5	60.00	20.00	20.00	3.00

The precursors were mixed together and pressed into parallelepiped shapes ($70 \times 70 \times 15$ mm) using a BERNARDO WK 10 TH hydraulic press (PWA HandelsgesmbH, Linz, Austria).

The firing process was conducted in a NABERTHERM 300–1300 °C electric furnace (Nabertherm GmbH, Lilienthal, Germany), considering a heating rate of $10 \text{ }^\circ\text{C}\cdot\text{min}^{-1}$ in the temperature range 20–550 °C and then $30 \text{ }^\circ\text{C}\cdot\text{min}^{-1}$ from 550 °C to the maximum firing temperatures: 700, 800, and 900 °C maintained for 90 min followed by cooling with $20 \text{ }^\circ\text{C}\cdot\text{min}^{-1}$ to room temperature was reached in order to avoid thermal stress. An image of the synthesized samples, before and after firing at 900 °C, is presented in Figure 2.

**Figure 2.** Glass ceramic samples before and after the heat treatment at 900 °C.

The dimensional stability was determined considering the volumetric shrinkage after firing, measured using an electronic caliper.

The samples' apparent density and apparent porosity were measured at 20 °C using the liquid saturation method under vacuum with deionized water as working liquid.

The total porosity of the studied samples was calculated using the relation (1):

$$P = \left(1 - \frac{\rho_S}{\rho_P}\right) \cdot 100 \text{ (\%)} \quad (1)$$

where: $\rho_S = \frac{m_S}{V_S}$ ($\text{g}\cdot\text{cm}^{-3}$) represents the bulk density of the parallelepiped shape sample having the mass m_S (g) and volume V_S (cm^3), and ρ_P represents the glass ceramic material density, measured using the pycnometer method using demineralized water as working liquid at 20 °C.

The glass ceramics' phase composition was investigated with a Rigaku Ultima 4 diffractometer (Rigaku Corp., Tokyo, Japan) using the monochromatic Cu- K_α radiation at an angular range of 5 to 80° for a scanning speed of $10^\circ\cdot\text{min}^{-1}$ at every 0.05 interval. XRD data were interpreted using PDXL software (Rigaku Corp., Tokyo, Japan); for the phase identification, we used PDF (Powder Diffraction File, PDF 2) cards according to the Joint Committee on Powder Diffraction Standards (JCPDS), International Centre for Diffraction Data (ICDD).

The microporous structure of the glass-ceramic matrices was analyzed by SEM, using a Quanta FEG 250 microscope (FEI Company, Hillsboro, OR, USA) using accelerating voltage of 20.0 kV in high vacuum mode.

The glass ceramics' chemical stability was estimated based on the dissolution rate (D_r) in deionized water calculated based on the relation (2):

$$D_r = \frac{m_i - m_f}{t} \quad (\mu\text{g h}^{-1}) \quad (2)$$

where: m_i is the initial sample mass, and m_f is the sample mass after t (28 days) immersed in 100 mL deionized water at a temperature of 20 °C and then dried until reaching constant mass in a laboratory oven at 110 °C.

The barium and lead ion immobilization in the studied glass-ceramic matrix was measured using leaching tests performed according to the American Extraction Procedure Toxicity Test [66]. Deionized water was used as extraction solvent at a constant temperature of 20 ± 2 °C, with ions leachability analysis being measured after 28 days using a Bruker Aurora ICP mass spectrometer (Bruker, Billerica, MA, USA).

The compression tests were performed using a Zwick Roell AllroundLine equipment (ZwickRoell Testing Systems GmbH, Fürstenfeld, Austria) with a 5–250 kN test load cell and a crosshead speed of $1.0 \text{ (mm} \cdot \text{min}^{-1})$. The samples were cut using a diamond saw in parallelepipedal shapes having $25 \times 25 \times 12$ mm in order to respect the length/height ratio of 1.5–2.5, as recommended by ASTM C1424-15 [67], and then polished to obtain highly parallel and smooth opposite bases surfaces.

3. Results and Discussion

3.1. Dimensional Stability after Heat Treatment

The physical-chemical transformations that take place in the masses studied during firing are accompanied by dimensional contractions. The measured shrinkage of the studied samples at the three heat treatment temperatures is illustrated in Figure 3.

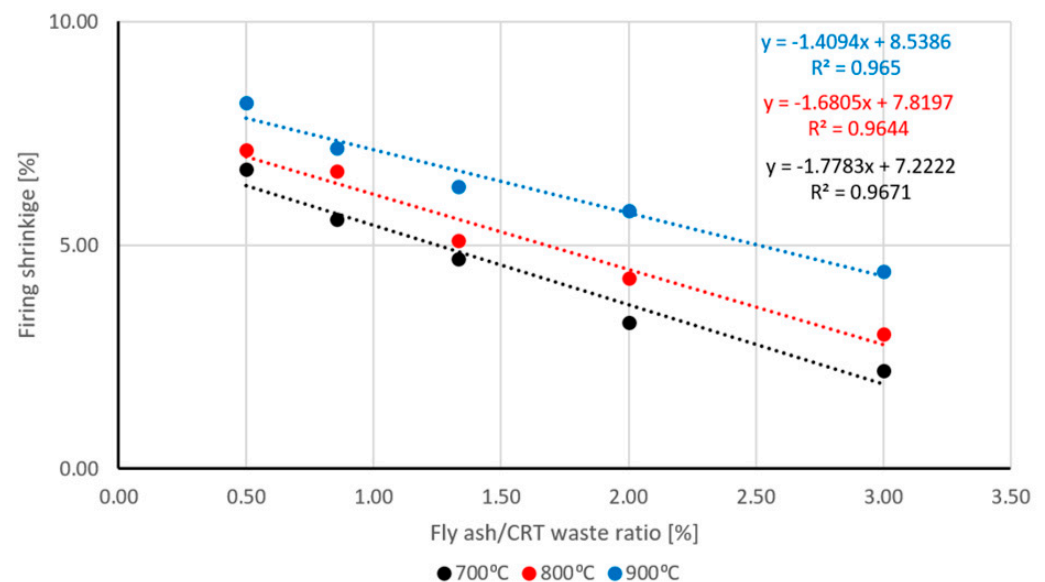
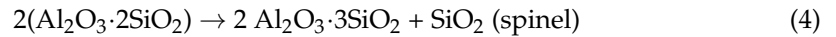
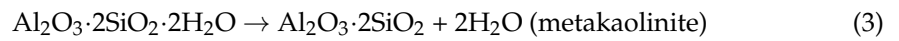


Figure 3. Evolution of the samples volumetric with composition.

The firing shrinkage increases with the increase of the heat treatment temperature, ranging between 2.19–6.70 % for the samples fired at 700 °C up to 4.42–8.18 % when the glass ceramics were fired at 900 °C, due to an increase of vitreous melt phase fluidity. This effect is more pronounced in the samples containing larger amounts of glass waste, corresponding to a lower fly ash/CRT waste ratio [68]. The evolution of samples' dimensional stability upon composition is quasilinear for all three synthesis temperatures, having the coefficient of determination ranging from 0.9644 up to 0.9671.

Replacing the kaolin with a waste mix leads to an increase in the dimensional stability of the samples by reducing the ceramic-specific contractions effect associated with

the kaolinite-metakaolinite-spinel-like structure and amorphous SiO₂ transformations (Equations (3) and (4)) [69]:



Reactions (3) and (4) occur at around 500 °C and 925 °C in pure kaolinitic masses [70]. The presence of the liquid phase favors the solid-state reactions, lowering the compounds' synthesis temperature.

3.2. Apparent Density, Apparent and Total Porosities

The influence of the fly ash/CRT waste ratio upon the apparent density and apparent porosity, measured at 20 °C using the liquid saturation method under vacuum using deionized water as a working liquid, is presented in Figure 4.

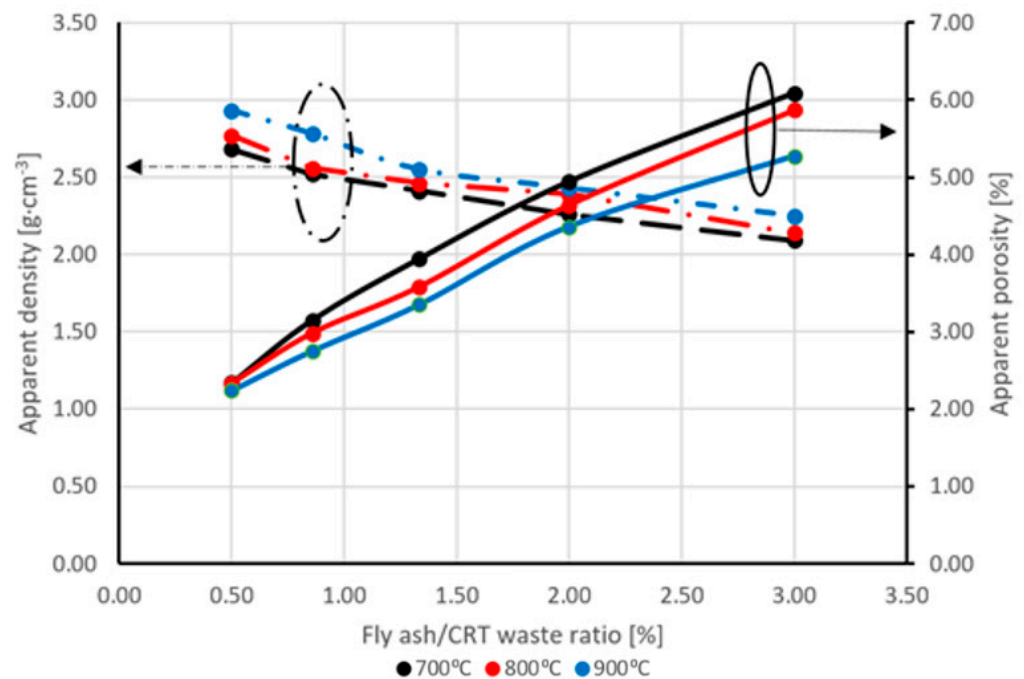


Figure 4. Evolution of the samples' apparent density and apparent porosity with composition.

The apparent density of the synthesized glass ceramics is affected by the heat treatment temperature, rising from 2.09–2.68 (g·cm⁻³) for the samples fired at 700 °C up to 2.25–2.93 (g·cm⁻³) for those fired at 900 °C. The apparent porosity decreases with the increase of the firing temperature of the samples from 2.34–6.08% at 700 °C down to 2.24–5.27% at 900 °C. This effect can be explained by considering the larger amounts of liquid phase generated as the heat treatment temperature increase, which fill the available pores, generating higher apparent densities and lower apparent porosities.

Larger quantities of fly ash, reflected by higher fly ash/CRT waste ratios, lead to lower apparent densities and higher apparent densities of the samples due to the foaming effect of the fly ash that generates gases during the heat treatment.

The total porosity of the obtained samples, calculated based on geometric considerations, decreased from 14.51–36.69% for the samples fired at 700 °C to 9.21–30.37% when the heat treatment was conducted at 900 °C. The influence of the two waste ratios upon the total and the apparent porosity of the synthesized samples is illustrated in Figure 5.

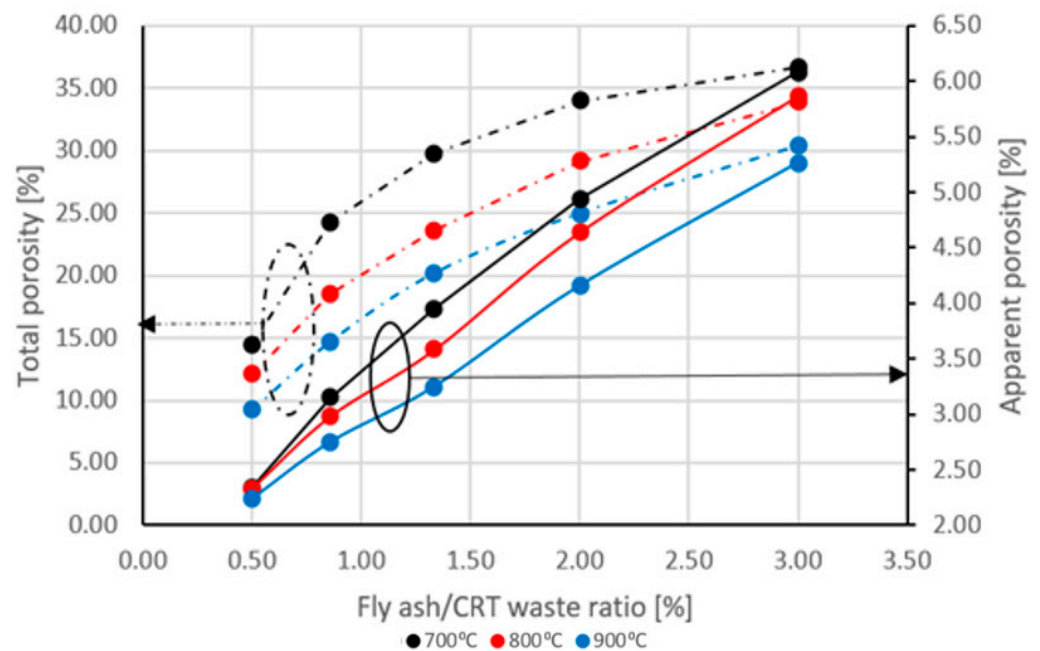


Figure 5. Composition influence upon the samples' closed porosity and apparent porosity.

The two types of porosity have a similar evolution with the fly ash/CRT waste ratio, considering the pore generation effect of the fly ash. The high firing temperature has a negative effect on both due to the higher amount of fluid phase generated by glass melting.

Considering the obtained values of the total and apparent porosities, it can be concluded that the majority of the pores in the glass ceramic matrix are closed, without communication with the samples' surfaces.

SEM images microstructure of samples 1 and 5 fired at 700 °C and 900 °C, respectively, are presented in Figure 6.

SEM images show the texture and microstructure differences between both samples of the same composition fired at the two considered temperatures and between samples of different compositions heat treated at the same temperature. The low waste amount in sample 1 leads to a textured surface with irregular pores having a scattered dimensional distribution (Figure 6A). A higher firing temperature favors pore coalescence, forming a small number of larger pores (Figure 6B). Changes in composition towards a higher waste amount in sample 5 generate a large number of small pores that are relatively evenly distributed on the samples' bodies (Figure 6C). Raising the heat treatment temperature to 900 °C (Figure 6D) generates a more textured surface with higher crystallinity and fewer pores.

3.3. Phase Composition

The phase analysis for samples 1 and 5 fired at the three considered temperatures is presented in Figure 7.

The main two phases present in both samples are quartz (JCPDS#01-083-0539) and anorthite (JCPDS#01-076-0948). The sharper quartz peak registered for sample 1 sintered at lower temperatures (Figure 7A) is caused by the larger kaolin amount used for its synthesis. No mullite-specific peaks were recorded due to the sintering temperature being too low. The broad shape of both spectra for the lower angular range is caused by the amorphous vitreous phase present in the glass ceramic structure [71].

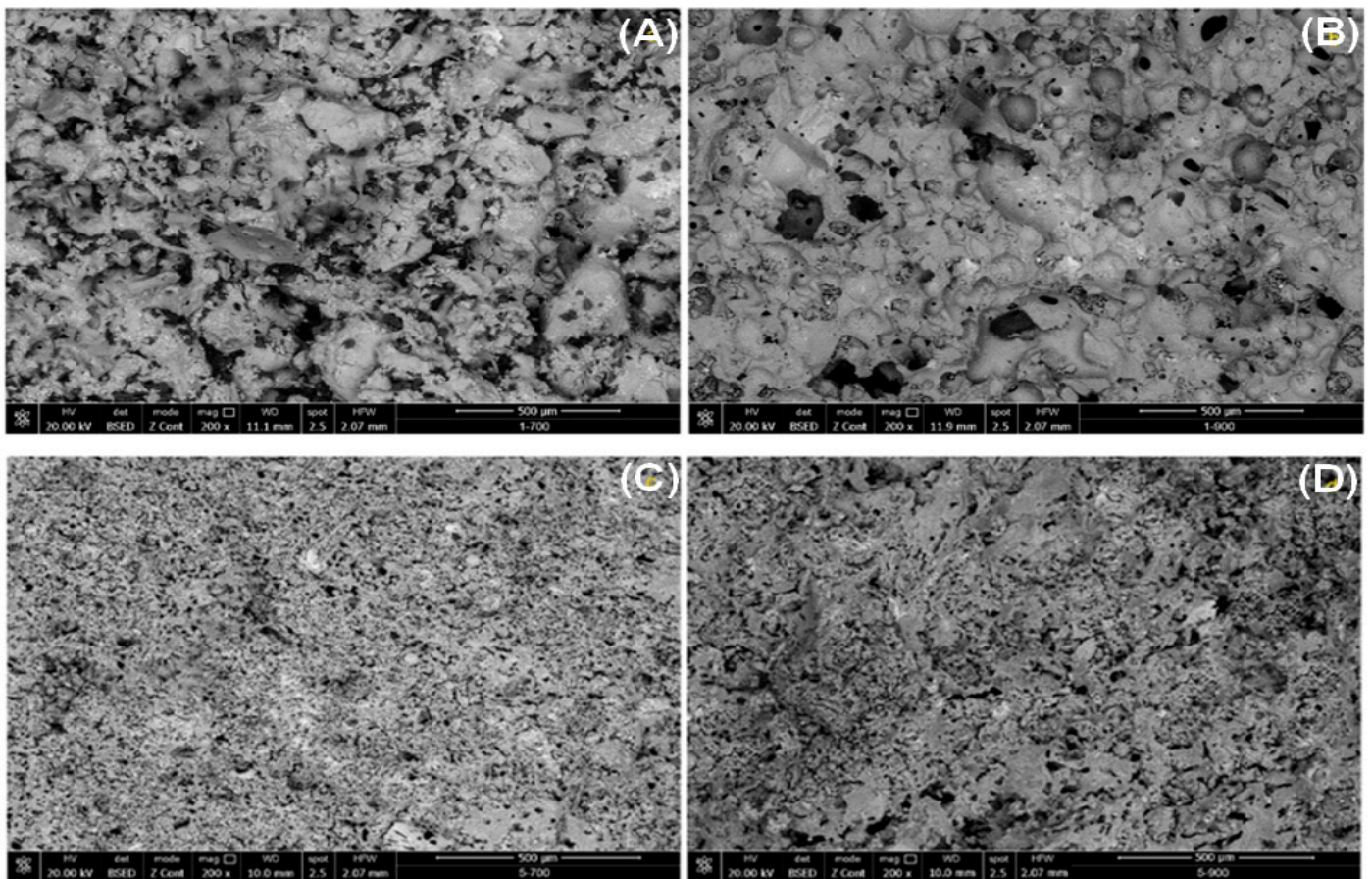


Figure 6. Microstructure of glass ceramics samples fired at different temperatures: (A) Sample 1—700 °C; (B) Sample 1—900 °C; (C) Sample 5—700 °C; (D) Sample 5—900 °C (cathode voltage 25 kV; working distance 10.0 mm, magnification 200×).

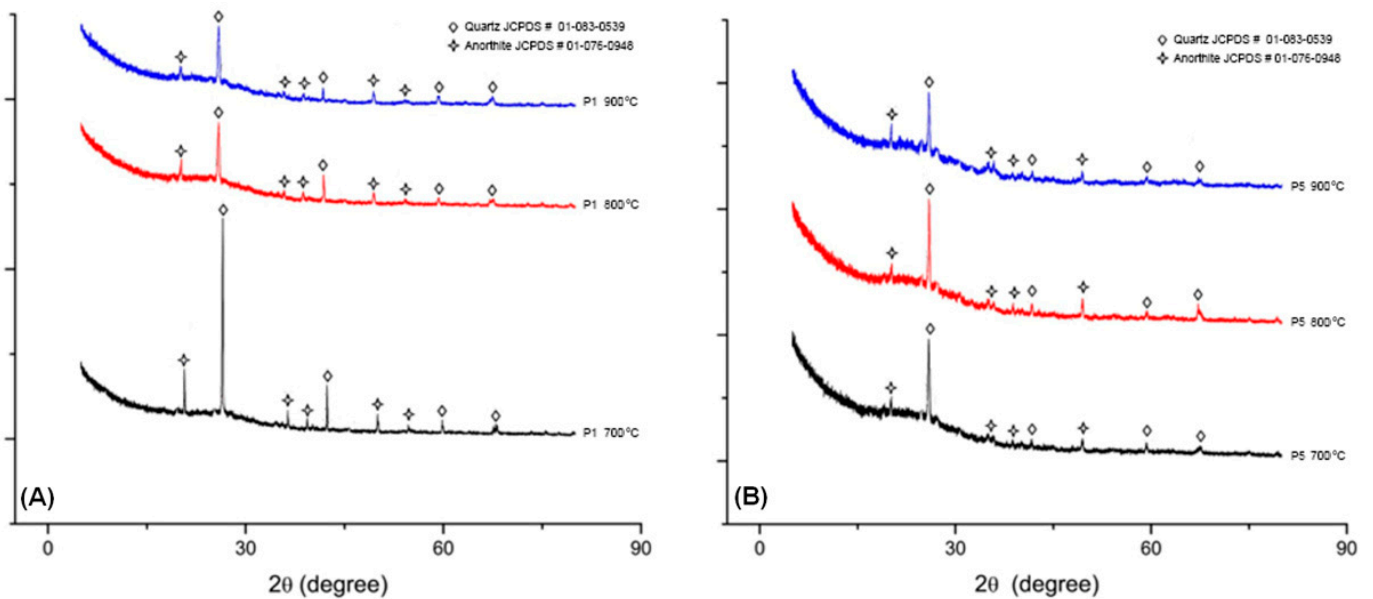


Figure 7. XRD patterns of samples 1 (A) and 5 (B) fired at 700 °C, 800 °C, and 900 °C.

3.4. Chemical Stability of the Samples

The chemical stability of the sintered glass ceramics, measured as samples dissolution rate after 28 days, is presented in Figure 8, together with the corresponding apparent porosity. All the samples show very good chemical stability; the dissolution rates decrease from 0.0115–0.0425 ($\mu\text{g}\cdot\text{h}^{-1}$) after firing at 700 °C down to 0.0035–0.0318 ($\mu\text{g}\cdot\text{h}^{-1}$) after firing at 900 °C. The most stable samples were obtained using the highest amount of CRT glass based on the encapsulating effect of the vitreous phase that protects the glass ceramic structure against the hydrolytic attack. Higher sintering temperatures favor this behavior by generating a more fluid phase that is able to coat all the exposed surfaces. The similar trend of the curves describing the chemical stability and the apparent porosity of the samples can be explained by considering the fact that the hydrolytic attack takes place in the open pores at the interface between the glass ceramic body and the attacking agent. Increasing the amount of fly ash used for the samples' synthesis decreased the chemical stability due to the foaming effect that generated more pores in the glass ceramic matrix.

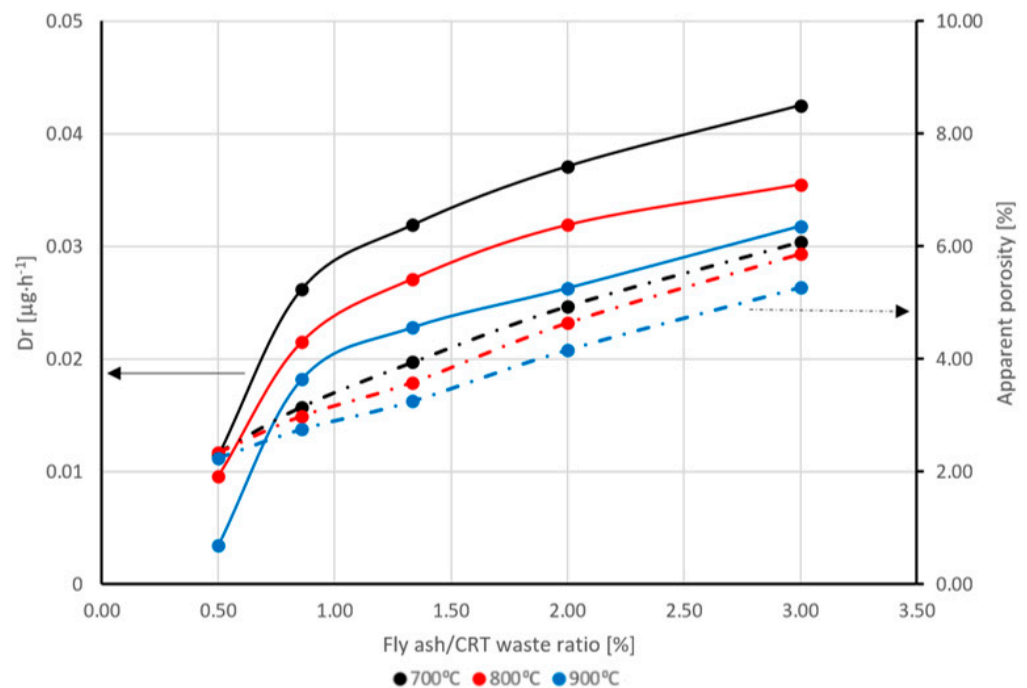


Figure 8. Composition influence upon the samples' dissolution rates and total porosity.

No barium or lead ion extractions from the sintered glass ceramics were determined after 28 days using the Bruker Aurora ICP-MS equipment. This behavior is caused by the fact that Ba^{2+} and Pb^{2+} ions are brought into the matrix structure via the CRT vitreous vector, less susceptible to hydrolytic attack.

3.5. Mechanical Properties of the Glass Ceramics

The obtained glass ceramic compositions are designed for outdoor ceramic pavements, and therefore, they must have good compressive strength. The effect of the glass ceramic composition upon the compression strength of the synthesized samples is illustrated in Figure 9 together with the samples' total porosity.

The compression strength of the samples rises from those sintered at 700 °C, ranging between 1.42–5.78 ($\text{N}\cdot\text{mm}^{-2}$) up to 4.09–11.83 ($\text{N}\cdot\text{mm}^{-2}$) for those obtained at 900 °C. The high sintering temperatures and the presence of kaolin have a positive effect on the compression behavior of the obtained samples considering that the mechanical strength of the glass ceramic matrix is based on the ceramic bonds formed at higher firing temperatures.

The increase in the total porosity generates structural discontinuities leading to a decrease in the samples' compression strength.

The measured compression strength was compared with the literature data for outdoor pavements in Table 3. The materials synthesized have a comparable compression strength to those reported by other researchers. It is worth noting that these previous results were obtained for both concrete and ceramic pavements, respectively, fired at temperatures above 1200 °C, which is much higher than the temperature used in the present study. The present study was focused on recycling waste in an economically efficient manner. It is known that higher sintering temperatures lead to better mechanical properties in the glass ceramic matrix, but they come at the cost of increased energy consumption and negative environmental impacts. The values obtained for porosity and compressive strength fit the synthesized materials as ceramic paving materials in accordance with the American Standards [72,73].

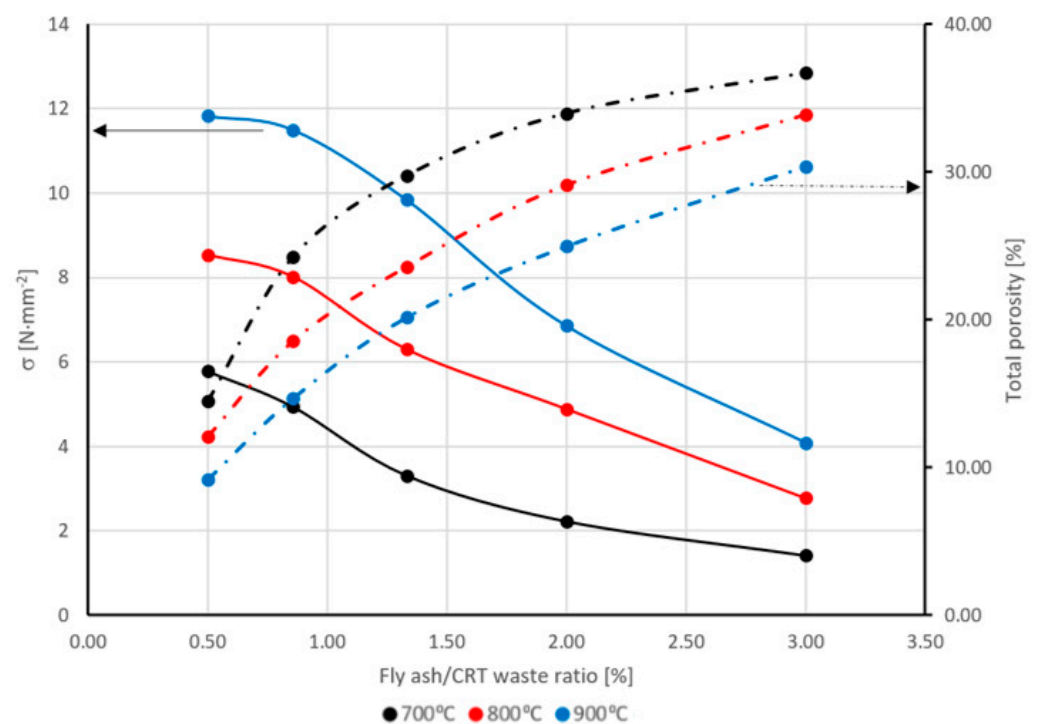


Figure 9. Composition influence upon the compression strength and total porosity.

Table 3. Comparison of the compression strength of the synthesized samples with other outdoor pavement materials mentioned in the literature.

Total Porosity (%)	Compression Strength (N·mm ⁻²)	Reference
3.0–29.0	4.68–15.08	[74]
12.1–13.5	43.90–62.40	[75]
8.0–24.0	52.67	[76]
18.6–20.40	25.67–31.26	[77]
15.0–20.0	3.50–27.50	[78]
9.2–36.7	1.42–11.83	This study

4. Conclusions

The present research proposes a new alternative for fly ash and cathode ray tube waste recycling for glass ceramics obtained using lower sintering temperatures in order to reduce energy consumption and environmental impacts. The main advantage of this method is that it immobilizes a hazardous waste, CRT, containing both lead and barium as a ceramic outdoor marketable pavement product.

The dimensional stability of the obtained material, expressed by the firing shrinkage range between 2.19–8.18%, is positively influenced by the waste mix/kaolin ratio due to a decrease in the ceramic-specific contractions effect associated with the kaolinite-metakaolinite-spinel transformations. The firing temperature negatively affects the dimensional stability due to the higher amount and fluidity of the glass melt generated as the temperature increases.

The apparent density of the obtained materials is positively affected by the heat treatment temperature, rising from 2.09 to 2.93 ($\text{g}\cdot\text{cm}^{-3}$), while the apparent porosity decreases with the increase of the firing temperature from 6.08 to 2.24 %. As the heat treatment temperature increases, larger amounts of liquid phase fill the available pores, generating higher apparent densities and lower apparent porosities.

The total porosity of the sintered materials, calculated based on geometric consideration, decreases from 36.69 to 9.21% as the heat treatment increases due to the pore-filling effect of the liquid phase. The total and apparent porosity obtained values suggest that the majority of the pores in the glass ceramic matrix are closed. SEM analysis shows the influence of the composition and firing temperatures on the materials' texture and microstructure. Higher firing temperatures generate a small number of larger pores, while higher waste amounts lead to a large number of small pores that are relatively evenly distributed on the samples' bodies.

The synthesized materials have very good chemical stability, the dissolution rates range between 0.0035–0.0425 ($\mu\text{g}\cdot\text{h}^{-1}$). The sintering temperature and the CRT waste amount have a positive effect on the chemical stability due to an encapsulating effect of the vitreous phase that protects the glass ceramic structure against the hydrolytic attack. The chemical stability and the apparent porosity of the samples show a similar evolution in relation to the composition confirming that the hydrolytic attack takes place in the open pores, at the interface between the glass ceramic body and the attacking agent.

Considering the hazardous character of the CRT waste the lead and barium leachability from the obtained matrix was measured. No barium or lead ions extraction was not highlighted after 28 days, which is explained by the fact that Ba^{2+} and Pb^{2+} ions came via the CRT glass that is stable to the hydrolytic attack.

The compression strength of the obtained samples ranges between 1.42–11.83 ($\text{N}\cdot\text{mm}^2$). The firing temperature and the presence of kaolin have a positive effect on the compression behavior, knowing that the mechanical strength of the glass ceramic matrix is based on the ceramic bonds, glass having a brittle behavior. The samples' porosity has a negative influence on the compression strength by generating structural discontinuities.

These results suggest the viability of the proposed solution to use fly ash and CRT waste together with kaolin to obtain glass ceramic materials with a high potential to be used as outdoor paving materials.

Supplementary Materials: The following supporting information can be downloaded at: <https://www.mdpi.com/article/10.3390/su15043021/s1>, Figure S1: Bojidar Kaolin RDX pattern; Figure S2: Fly ash RDX pattern.

Author Contributions: Conceptualization, C.V., G.M. and S.P.; methodology, C.V., G.M. and M.D.; software, C.V. and G.M.; validation, C.V., G.M. and M.D.; formal analysis, C.V., G.M. and S.P.; investigation, C.V., G.M., S.P., M.D. and S.B.; resources, C.V. and M.D.; data curation, C.V.; writing—original draft preparation, C.V., G.M., S.P. and S.B.; writing—review and editing, C.V., G.M., S.P. and M.D.; visualization, C.V.; supervision, C.V. All authors have read and agreed to the published version of the manuscript.

Funding: This research received no external funding.

Institutional Review Board Statement: Not applicable.

Informed Consent Statement: Not applicable.

Data Availability Statement: All the experimental data obtained are presented, in the form of tables and/or figures, in the article.

Conflicts of Interest: The authors declare no conflict of interest.

References

- Dhir, A.; Koshta, N.; Goyal, R.K.; Sakashita, M.; Almotairi, M. Behavioral reasoning theory (BRT) perspectives on E-waste recycling and management. *J. Clean. Prod.* **2021**, *280*, 124269. [[CrossRef](#)]
- Ahirwar, R.; Tripathi, A.K. E-waste management: A review of recycling process, environmental and occupational health hazards, and potential solutions. *Environ. Nanotechnol. Monit. Manag.* **2021**, *15*, 100409. [[CrossRef](#)]
- Aboelmegeed, M. E-waste recycling behaviour: An integration of recycling habits into the theory of planned behavior. *J. Clean. Prod.* **2021**, *278*, 124182. [[CrossRef](#)]
- Shevchenko, T.; Laitala, K.; Danko, Y. Understanding Consumer E-Waste Recycling Behavior: Introducing a New Economic Incentive to Increase the Collection Rates. *Sustainability* **2019**, *11*, 2656. [[CrossRef](#)]
- Kuehr, R. 1—Global e-waste initiatives. In *Woodhead Publishing Series in Electronic and Optical Materials, Waste Electrical and Electronic Equipment (WEEE) Hand-Book*; Goodship, V., Stevels, A., Eds.; Woodhead Publishing: Cambridge, UK, 2012; pp. 3–16.
- Wang, B.; Ren, C.; Dong, X.; Zhang, B.L.; Wang, Z. Determinants shaping willingness towards on-line recycling behaviour: An empirical study of household e-waste recycling in China. *Resour. Conserv. Recycl.* **2019**, *143*, 218–225. [[CrossRef](#)]
- Forti, V.; Balde, C.P.; Kuehr, R.; Bel, G. *The Global E-Waste Monitor 2020: Quantities, Flows and the Circular Economy Potential*; United Nations University/United Nations Institute for Training and Research, International Telecommunication Union, and International Solid Waste Association: Bonn, Germany, 2020.
- Shevchenko, T.; Saidani, M.; Danko, Y.; Golysheva, I.; Chovancová, J.; Vavrek, R. Towards a Smart E-Waste System Utilizing Supply Chain Participants and Interactive Online Maps. *Recycling* **2021**, *6*, 8. [[CrossRef](#)]
- Chi, X.; Wang, M.Y.L.; Reuter, M.A. E-waste collection channels and household recycling behaviors in Taizhou of China. *J. Clean. Prod.* **2014**, *80*, 87–95. [[CrossRef](#)]
- Baron, Y.; Majjala, A.; Lopez, V.; Thiebaut, E.; Haarman, A.; Kaartinen, H.; Herreras, L.; Hajosi, E.; Wuisan, L.; Winkler, J.; et al. The CEWASTE Assurance and Verification System for the Certification of Waste Management Operators with CRM Focused Requirements. In Proceedings of the Electronic Goes Green, Berlin, Germany, 1 September 2020.
- Kurtuluş, R.; Kavas, T.; Kavas, T.; Tekin, H.O.; Kurucu, Y. Synthesis and characterization of waste CRT glasses through physical, optical and structural properties: A comprehensive study on recycling. *Optik* **2021**, *248*, 168167. [[CrossRef](#)]
- Yao, Z.; Ling, T.K.; Sarker, P.K.; Su, W.; Liu, J.; Wu, W.; Tang, J. Recycling difficult-to-treat e-waste cathode-ray-tube glass as construction and building materials: A critical review. *Renew. Sustain. Energy Rev.* **2018**, *81*, 595–604. [[CrossRef](#)]
- Paunescu, L.; Dragoescu, M.F.; Axinte, S.M.; Cosmulescu, F. Nonconventional manufacture technique of cellular glass from recycled aluminosilicate glass-based waste. *Mater. Sci. Eng. Int. J.* **2021**, *5*, 11–16.
- Smolii, V.A.; Kosarev, A.S.; Yatsenko, E.A. Porophores for Cellular Glass Based on TPP Ash-Slag Materials. *Glass Ceram.* **2020**, *77*, 94–97. [[CrossRef](#)]
- Praxedes, F.M.; Teixeira, J.V.U.; Da Luz, P.T.S.; Fernandez, O.J.C.; Figueira, B.A.M.; de Oliveira Araújo, S.M.S. Use of industrial residues for production of cellular glasses of low environmental impact. *Mater. Res. Express* **2019**, *6*, 065513. [[CrossRef](#)]
- Yuan, H.; Wu, H.; Guan, J. Synthesis of foam glass-ceramic from CRT panel glass using one-step powder sintering. *IOP Conf. Ser. Earth Environ. Sci.* **2018**, *186*, 012020. [[CrossRef](#)]
- Xu, B.; Wang, F.; Yang, J.; Yang, B.; Zhao, J. Enhancing Pb Removal and Synthesizing Glass-Ceramics from Waste CRTs Funnel Glass by Red Mud. *J. Sustain. Metall.* **2020**, *6*, 367–374. [[CrossRef](#)]
- Zhang, Q.; He, F.; Shu, H.; Qiao, Y.; Mei, S.; Jin, M.; Xie, J. Preparation of high strength glass ceramic foams from waste cathode ray tube and germanium tailings. *Constr. Build. Mater.* **2016**, *111*, 105–110. [[CrossRef](#)]
- Lv, J.; Yang, H.; Jin, Z.; Zhao, M. Lead extraction and glass-ceramics synthesis from waste cathode ray tube funnel glass through cooperative smelting process with coal fly ash. *Waste Manag.* **2018**, *76*, 687–696. [[CrossRef](#)]
- Lu, X.; Yang, J.; Ning, X.A.; Shih, K.; Wang, F. Crystallization pathways in glass-ceramics by sintering cathode ray tube (CRT) glass with kaolin-based precursors. *J. Eur. Ceram. Soc.* **2018**, *38*, 5184–5191. [[CrossRef](#)]
- Revelo, R.J.; Menegazzo, A.P.; Ferreira, E.B. Cathode-Ray Tube panel glass replaces frit in transparent glazes for ceramic tiles. *Ceram. Int.* **2018**, *44*, 13790–13796. [[CrossRef](#)]
- Reben, M.; Kosmal, M.; Pałczyńska, N.; Pichniarczyk, P. Waste immobilization and environmental sustainability in glass-ceramics glazes development. *E3S Web Conf.* **2016**, *10*, 00071. [[CrossRef](#)]
- Mourou, C.; Martín-Morales, M.; Zamorano, M.; Ruiz, D.P. Light Reflectance Characterization of Waste Glass Coating for Tiles. *Appl. Sci.* **2022**, *12*, 1537. [[CrossRef](#)]
- Qi, Y.; Xiao, X.; Lu, Y.; Shu, J.; Wang, J.; Chen, M. Cathode ray tubes glass recycling: A review. *Sci. Total Environ.* **2019**, *650*, 2842–2849. [[CrossRef](#)] [[PubMed](#)]
- Bernardo, E.; Esposito, L.; Rambaldi, E.; Tucci, A. Glass based stoneware as a promising route for the recycling of waste glasses. *Adv. Appl. Ceram.* **2009**, *108*, 2–8. [[CrossRef](#)]
- Gopal, P.M.; Soorya Prakash, K. Wire electric discharge machining of silica rich E-waste CRT and BN reinforced hybrid magnesium MMC. *Silicon* **2019**, *11*, 1429–1440.
- Rana, V.; Kumar, H.; Kumar, A. Fabrication of hybrid metal matrix composites (HMMCs)—A review of comprehensive research studies. *Mater. Today Proc.* **2022**, *56*, 3102–3107. [[CrossRef](#)]

28. Taurino, R.; Bondioli, F.; Messori, M. Use of different kinds of waste in the construction of new polymer composites: Review. *Mater. Today Sustain.* **2023**, *21*, 100298. [[CrossRef](#)]
29. Popovici, A.; Corbu, O.; Popita, G.E.; Rosu, C.; Proorocu, M.; Sandu, A.V.; Abdullah, M.M.A.B. Modern mortars with electronic waste scraps (glass and plastic). *Mater. Plast.* **2015**, *52*, 588–592.
30. Naganathan, S.; Silvadanam, S.; Chung, T.Y.; Nicolasselvam, M.F.; Thiruchelvam, S. Use of wastes in developing mortar—A review. *Adv. Mater. Res.* **2014**, *935*, 146–150. [[CrossRef](#)]
31. Long, W.J.; Gu, Y.C.; Xing, F.; Khayat, K.H. Evaluation of the inhibiting effect of graphene oxide on lead leaching from waste cathode-ray tube glass incorporated in cement mortar. *Cem. Concr. Compos.* **2019**, *104*, 103337. [[CrossRef](#)]
32. Luhar, S.; Luhar, I. Potential application of E-wastes in construction industry: A review. *Constr. Build. Mater.* **2019**, *203*, 222–240. [[CrossRef](#)]
33. Liu, T.; Song, W.; Zou, D.; Li, L. Dynamic mechanical analysis of cement mortar prepared with recycled cathode ray tube (CRT) glass as fine aggregate. *J. Clean. Prod.* **2018**, *174*, 1436–1443. [[CrossRef](#)]
34. Ling, T.C.; Poon, C.S.; Lam, W.S.; Chan, T.P.; Fung, K.K.L. Utilization of recycled cathode ray tubes glass in cement mortar for X-ray radiation-shielding applications. *J. Hazard. Mater.* **2012**, *199*, 321–327. [[CrossRef](#)] [[PubMed](#)]
35. Zhao, H.; Poon, C.S. Recycle of large amount cathode ray tube funnel glass sand to mortar with supplementary cementitious materials. *Constr. Build. Mater.* **2021**, *308*, 124953. [[CrossRef](#)]
36. Zacco, A.; Borgese, L.; Gianoncelli, A.; Struis, R.P.; Depero, L.E.; Bontempi, E. Review of fly ash inertisation treatments and recycling. *Environ. Chem. Lett.* **2014**, *12*, 153–175. [[CrossRef](#)]
37. Yao, Z.T.; Ji, X.S.; Sarker, P.K.; Tang, J.H.; Ge, L.Q.; Xia, M.S.; Xi, Y.Q. A comprehensive review on the applications of coal fly ash. *Earth. Sc. Rev.* **2015**, *141*, 105–121. [[CrossRef](#)]
38. Kurda, R.; de Brito, J.; Silvestre, J.D. A comparative study of the mechanical and life cycle assessment of high-content fly ash and recycled aggregates concrete. *J. Build. Eng.* **2020**, *29*, 101173. [[CrossRef](#)]
39. Tošić, N.; Marinković, S.; Pecić, N.; Ignjatović, I.; Dragaš, J. Long-term behaviour of reinforced beams made with natural or recycled aggregate concrete and high-volume fly ash concrete. *Constr. Build. Mater.* **2018**, *176*, 344–358. [[CrossRef](#)]
40. Kurda, R.; de Brito, J.; Silvestre, J.D. Water absorption and electrical resistivity of concrete with recycled concrete aggregates and fly ash. *Cem. Concr. Compos.* **2019**, *95*, 169–182. [[CrossRef](#)]
41. Kurda, R.; de Brito, J.; Silvestre, J.D. Combined economic and mechanical performance optimization of recycled aggregate concrete with high volume of fly ash. *Appl. Sci.* **2018**, *8*, 1189. [[CrossRef](#)]
42. Pandey, V.C.; Singh, N. Impact of fly ash incorporation in soil systems. *Agric. Ecosyst. Environ.* **2010**, *136*, 16–27. [[CrossRef](#)]
43. Shaheen, S.M.; Hooda, P.S.; Tsadilas, C.D. Opportunities and challenges in the use of coal fly ash for soil improvements—A review. *J. Environ. Manag.* **2014**, *145*, 249–267. [[CrossRef](#)]
44. Sahu, G.; Bag, A.G.; Chatterjee, N.; Mukherjee, A.K. Potential use of fly ash in agriculture: A way to improve soil health. *J. Pharmacogn. Phytochem.* **2017**, *6*, 873–880.
45. Hoy, M.; Horpibulsuk, S.; Arulrajah, A. Strength development of Recycled Asphalt Pavement—Fly ash geopolymer as a road construction material. *Constr. Build. Mater.* **2016**, *117*, 209–219. [[CrossRef](#)]
46. Poltue, T.; Suddepong, A.; Horpibulsuk, S.; Samingthong, W.; Arulrajah, A.; Rashid, A.S.A. Strength development of recycled concrete aggregate stabilized with fly ash-rice husk ash based geopolymer as pavement base material. *Road Mater. Pavement Des.* **2020**, *21*, 2344–2355. [[CrossRef](#)]
47. Lu, Y.; Tian, A.; Zhang, J.; Tang, Y.; Shi, P.; Tang, Q.; Huang, Y. Physical and chemical properties, pretreatment, and recycling of municipal solid waste incineration fly ash and bottom ash for highway engineering: A literature review. *Adv. Civ. Eng.* **2020**, *2020*, 8886134. [[CrossRef](#)]
48. Liu, J.; Dong, Y.; Dong, X.; Hampshire, S.; Zhu, L.; Zhu, Z.; Li, L. Feasible recycling of industrial waste coal fly ash for preparation of anorthite-cordierite based porous ceramic membrane supports with addition of dolomite. *J. Eur. Ceram. Soc.* **2016**, *36*, 1059–1071. [[CrossRef](#)]
49. Yuan, Q.; Robert, D.; Mohajerani, A.; Tran, P.; Pramanik, B.K. Utilisation of waste-to-energy fly ash in ceramic tiles. *Constr. Build. Mater.* **2022**, *347*, 128475. [[CrossRef](#)]
50. Jordán, M.M.; Montero, M.A.; Pardo-Fabregat, F. Technological behaviour and leaching tests in ceramic tile bodies obtained by recycling of copper slag and MSW fly ash wastes. *J. Mater. Cycles.* **2021**, *23*, 707–716. [[CrossRef](#)]
51. Yuan, N.; Zhang, X.; Zhao, A.; Tan, K.; Cui, Y. High-alumina fly ash as sustainable aluminum sources for the in situ preparation of Al-based eco-MOFs. *Colloids Surf. A Physicochem. Eng. Asp.* **2022**, *640*, 128421. [[CrossRef](#)]
52. Chen, T.; Yuan, N.; Wang, S.; Hao, X.; Zhang, X.; Wang, D.; Yang, X. The Effect of Bottom Ash Ball-Milling Time on Properties of Controlled Low-Strength Material Using Multi-Component Coal-Based Solid Wastes. *Sustainability* **2022**, *14*, 9949. [[CrossRef](#)]
53. Cao, G.; Yang, L.; Yuan, G.; Hu, J.; Shao, G.; Yan, L. Chemical diversity of iron species and structure evolution during the oxidation of C14 Laves phase Zr(Fe,Nb)₂ in subcritical environment. *Corros. Sci.* **2020**, *162*, 108218. [[CrossRef](#)]
54. Cao, G.; Yun, Y.; Xu, H.; Yuan, G.; Hu, J.; Shao, G. A mechanism assessment for the anti-corrosion of zirconia coating under the condition of subcritical water corrosion. *Corros. Sci.* **2019**, *152*, 54–59. [[CrossRef](#)]
55. Feng, N.; Chen, C.; Hu, J.; Shao, G.; Yuan, G.; Cao, G. Microstructural and mechanical evolution of amorphous Zr-Si with irradiation induced atomic reconfiguration and free volume variation. *Surf. Interfaces* **2022**, *30*, 101890. [[CrossRef](#)]

56. Belviso, C. State-of-the-art applications of fly ash from coal and biomass: A focus on zeolite synthesis processes and issues. *Prog. Energy Combust. Sci.* **2018**, *65*, 109–135. [[CrossRef](#)]
57. Panek, R.; Madej, J.; Bandura, L.; Słowik, G. Recycling of waste solution after hydrothermal conversion of fly ash on a semi-technical scale for zeolite synthesis. *Materials* **2021**, *14*, 1413. [[CrossRef](#)] [[PubMed](#)]
58. Supelano, G.I.; Cuaspuud, J.G.; Moreno-Aldana, L.C.; Ortiz, C.; Trujillo, C.A.; Palacio, C.A.; Parra Vargas, C.A.; Gómez, J.M. Synthesis of magnetic zeolites from recycled fly ash for adsorption of methylene blue. *Fuel* **2020**, *263*, 116800. [[CrossRef](#)]
59. Ju, S.; Yoon, J.; Sung, D.; Pyo, S. Mechanical properties of coal ash particle-reinforced recycled plastic-based composites for sustainable railway sleepers. *Polymers* **2020**, *12*, 2287. [[CrossRef](#)] [[PubMed](#)]
60. Nasir, N.H.M.; Usman, F.; Saggaf, A. Development of composite material from Recycled Polyethylene Terephthalate and fly ash: Four decades progress review. *Curr. Res. Green Sustain. Chem.* **2022**, *5*, 100280. [[CrossRef](#)]
61. Anandhan, S. Recent trends in fly ash utilization in polymer composites. *Int. J. Waste Resour.* **2014**, *4*, 1000149.
62. Long, W.J.; Zhang, X.; Xie, J.; Kou, S.; Luo, Q.; Wei, J.; Lin, C.; Feng, G.L. Recycling of waste cathode ray tube glass through fly ash-slag geopolymer mortar. *Constr. Build. Mater.* **2022**, *322*, 126454. [[CrossRef](#)]
63. Liang, B.; Zhang, M.; Li, H.; Zhao, M.; Xu, P.; Deng, L. Preparation of ceramic foams from ceramic tile polishing waste and fly ash without added foaming agent. *Ceram. Int.* **2021**, *47*, 23338–23349. [[CrossRef](#)]
64. Fan, Y.; Li, S.; Li, Y.; Liang, H.; Tang, M.; Huang, K.; Zhu, L. Recycling of municipal solid waste incineration fly ash in foam ceramic materials for exterior building walls. *J. Build. Eng.* **2021**, *44*, 103427. [[CrossRef](#)]
65. Rabelo Monich, P.; Lucas, H.; Friedrich, B.; Bernardo, E. Recyclable Porous Glass-Ceramics from the Smelting of MSWI Bottom Ash. *Ceramics* **2021**, *4*, 1–11. [[CrossRef](#)]
66. US EPA. *Extraction Procedure Toxicity Test in: Stabilization/Solidification of CERCLA and RCRA Wastes, US EPA625/6-89/022*; US EPA: Cincinnati, OH, USA, 1986.
67. *ASTM C1424-15*; Standard Test Method for Monotonic Compressive Strength of Advanced Ceramics at Ambient Temperature Advanced Concrete Technology and its Structural Applications. ASTM International: West Conshohocken, PA, USA, 2019.
68. Abubakar, M.; Muthuraja, A.; Rajak, D.K.; Ahmad, N.; Pruncu, C.I.; Lamberti, L.; Kumar, A. Influence of Firing Temperature on the Physical, Thermal and Microstructural Properties of Kankara Kaolin Clay: A Preliminary Investigation. *Materials* **2020**, *13*, 1872. [[CrossRef](#)] [[PubMed](#)]
69. Garcia-Valles, M.; Cuevas, D.; Alfonso, P.; Martínez, S. Thermal behaviour of ceramics obtained from the kaolinitic clays of Terra Alta, Catalonia, Spain. *J. Therm. Anal. Calorim.* **2022**, *147*, 5303–5312. [[CrossRef](#)]
70. Valášková, M.; Blahůšková, V.; Vlček, J. Effects of Kaolin Additives in Fly Ash on Sintering and Properties of Mullite Ceramics. *Minerals* **2021**, *11*, 887. [[CrossRef](#)]
71. Krstić, I.; Zec, S.; Lazarević, V.; Stanisavljević, M.; Golubović, T. Use of sintering to immobilize toxic metals present in galvanic sludge into a stable glass-ceramic structure. *Sci. Sinter.* **2018**, *50*, 139–147. [[CrossRef](#)]
72. *ASTM C1272*; Standard Specification for Heavy Vehicular Paving Brick. ASTM International: West Conshohocken, PA, USA, 2014.
73. *ASTM C902*; Standard Specification for Pedestrian and Light Traffic Paving Brick. ASTM International: West Conshohocken, PA, USA, 2014.
74. Chopra, M.; Wanielista, M.; Mulligan, A.M. *Compressive Strength of Pervious Concrete Pavements*; Final Report; Stormwater Management Academy, University of Central Florida: Orlando, FL, USA, January 2007.
75. Penteadó, C.S.G.; de Carvalho, E.V.; Lintz, R.C.C. Reusing ceramic tile polishing waste in paving block manufacturing. *J. Clean. Prod.* **2015**, *112*, 514–520. [[CrossRef](#)]
76. Rozenstrauha, I.; Sosins, G.; Petersone, L.; Krage, L.; Drille, M.; Filipenkov, V. Production of glass-ceramics from sewage sludge and waste glass. *IOP Conf. Ser. Mater. Sci. Eng.* **2011**, *25*, 012016. [[CrossRef](#)]
77. Montaev, S.A.; Zharylgapov, S.M.; Montaeva, N.S.; Shakeshev, B.T. Research of possibility of producing ceramic paving stones by vibrocompression with the purpose of using them in the improvement of urban areas. *IOP Conf. Ser. Mater. Sci. Eng.* **2020**, *775*, 012118. [[CrossRef](#)]
78. Prahara, E.; Meilani. Compressive Strength and Water Absorption of Pervious Concrete that Using the Fragments of Ceramics and Roof Tiles. *EPJ Web Conf.* **2014**, *68*, 00015. [[CrossRef](#)]

Disclaimer/Publisher's Note: The statements, opinions and data contained in all publications are solely those of the individual author(s) and contributor(s) and not of MDPI and/or the editor(s). MDPI and/or the editor(s) disclaim responsibility for any injury to people or property resulting from any ideas, methods, instructions or products referred to in the content.